RTEL-1 Enforces Meiotic Crossover Interference and Homeostasis

Jillian L. Youds, *et al.*

Science **327**, 1254 (2010);
DOI: 10.1126/science.1183112

0.0001; Fig. 4, B and D; WT, 79.54 ± 2.03%, n = 11, $P < 0.0001$). To address the possibility that the DHPG-mediated depotentiation could be due in part to astrocyte Ca^{2+}, we performed the same experiments using IP_3R2 KO mice. The magnitude of DHPG-induced depotentiation in IP_3R2 KO slices was not only significant ($P < 0.0001$), it was also similar to the magnitude of depotentiation that was recorded in WT littermate slices ($P = 0.43$), indicating that depotentiation does not rely, even in part, on Ca^{2+}-dependent gliotransmitter release from astrocytes (Fig. 4, C and D; IP_3R2 KO, 66.95 ± 2.79%, n = 6; WT, 72.70 ± 5.72%, n = 8). These results demonstrate and confirm previous data that DHPG-induced modulation of neuronal activity (*28*, *29*), such as depotentiation (*26*), is due to the direct action of DHPG on neuronal group I mGluRs (*26*), and not to astrocytic group I mGluR-mediated Ca^{2+} elevations and putative gliotransmitter release.

We provide here strong evidence that G_q GPCR Ca^{2+} signaling in astrocytes does not affect spontaneous and evoked excitatory action potential (AP)-mediated synaptic transmission or short- and long-term plasticity at the SC-CA1 synapse. We used two molecular tools (the $MrgA1^+$ and IP_3R2 KO mouse models), as well as the activation of endogenous astrocytic G_q GPCRs, to manipulate Ca^{2+} in astrocytes. A battery of eight electrophysiological protocols (sEPSCs, NMDA eEPSCs, evoked AMPA fEPSPs, I/O curves, PPF, PTP, and two forms of LTP) were studied, all of which point to a lack of modulation of excitatory AP-mediated synaptic transmission by astrocytic G_q GPCR Ca^{2+} signaling. The most logical conclusion from the present analysis is that astrocytic G_q GPCRs and Ca^{2+} signaling activity are not tied to the release of gliotransmitters affecting synaptic transmission or short and long-term plasticity. Therefore, our results suggest that gliotransmission reflects the pharmacological approaches that were used in previous studies (*3*–*10*, *12*) and, at least within the hippocampus, does not occur when the endogenous regulators of astrocyte Ca^{2+}, the G_q GPCRs, or the IP_3R2 themselves are stimulated or inactivated in a cellular-selective manner. These findings suggest that the mechanisms of gliotransmitter release should be reconsidered. These results have profound implications for our understanding of synaptic transmission and should affect the interpretation of a broad range of findings. Thus, the purpose of neuron-to-astrocyte G_q GPCR Ca^{2+} signaling in neurophysiology remains an open question.

References and Notes

1. X. Wang *et al.*, *Nat. Neurosci.* **9**, 816 (2006).
2. J. T. Porter, K. D. McCarthy, *J. Neurosci.* **16**, 5073 (1996).
3. M. C. Angulo, A. S. Kozlov, S. Charpak, E. Audinat, *J. Neurosci.* **24**, 6920 (2004).
4. T. Fellin *et al.*, *Neuron* **43**, 729 (2004).
5. C. J. Lee *et al.*, *J. Physiol.* **581**, 1057 (2007).
6. M. Navarrete, A. Araque, *Neuron* **57**, 883 (2008).
7. L. Pasti, A. Volterra, T. Pozzan, G. Carmignoto, *J. Neurosci.* **17**, 7817 (1997).
8. G. Perea, A. Araque, *J. Neurosci.* **25**, 2192 (2005).
9. E. Shigetomi, D. N. Bowser, M. V. Sofroniew, B. S. Khakh, *J. Neurosci.* **28**, 6659 (2008).
10. G. Perea, A. Araque, *Science* **317**, 1083 (2007).
11. A. Serrano, N. Haddjeri, J. C. Lacaille, R. Robitaille, *J. Neurosci.* **26**, 5370 (2006).
12. C. Agulhon *et al.*, *Neuron* **59**, 932 (2008).
13. T. A. Fiacco *et al.*, *Neuron* **54**, 611 (2007).
14. T. A. Fiacco, C. Agulhon, K. D. McCarthy, *Annu. Rev. Pharmacol. Toxicol.* **49**, 151 (2009).
15. N. X. Tritsch, D. E. Bergles, *Neuron* **54**, 497 (2007).
16. J. Petravicz, T. A. Fiacco, K. D. McCarthy, *J. Neurosci.* **28**, 4967 (2008).
17. X. Li, A. V. Zima, F. Sheikh, L. A. Blatter, J. Chen, *Circ. Res.* **96**, 1274 (2005).
18. Y. Sasaki *et al.*, *J. Neurochem.* **68**, 2194 (1997).
19. M. Andersson, F. Blomstrand, E. Hanse, *J. Physiol.* **585**, 843 (2007).
20. T. A. Fiacco, K. D. McCarthy, *J. Neurosci.* **24**, 722 (2004).
21. O. Pascual *et al.*, *Science* **310**, 113 (2005).
22. R. S. Zucker, *Neuron* **17**, 1049 (1996).
23. H. J. Chung *et al.*, *Proc. Natl. Acad. Sci. U.S.A.* **106**, 635 (2009).
24. C. C. Huang, Y. C. Liang, K. S. Hsu, *J. Biol. Chem.* **276**, 48108 (2001).
25. R. Li, F. S. Huang, A. K. Abbas, H. Wigström, *BMC Neurosci.* **8**, 55 (2007).
26. W. M. Zho, J. L. You, C. C. Huang, K. S. Hsu, *J. Neurosci.* **22**, 8838 (2002).
27. Y. Izumi, C. F. Zorumski, *J. Neurosci.* **28**, 9557 (2008).
28. G. Mannaioni, M. J. Marino, O. Valenti, S. F. Traynelis, P. J. Conn, *J. Neurosci.* **21**, 5925 (2001).
29. M. G. Rae, A. J. Irving, *Neuropharmacology* **46**, 1057 (2004).

30. We thank K. Casper for making $MrgA1^+$ mice; J. Chen for providing IP_3R2 KO mice; and B. Djukic, B. Philpot, A. Roberts, and J. de Marchena for valuable help and discussions. This work was supported by NIH grants NS033938 and NS020212.

Supporting Online Material

www.sciencemag.org/cgi/content/full/327/5970/1250/DC1
Materials and Methods
SOM Text S1 to S14
Figs. S1 to S3
References
Movie S1

17 November 2009; accepted 19 January 2010
10.1126/science.1184821

RTEL-1 Enforces Meiotic Crossover Interference and Homeostasis

Jillian L. Youds,[1] David G. Mets,[2] Michael J. McIlwraith,[3] Julie S. Martin,[1] Jordan D. Ward,[1]* Nigel J. ONeil,[4] Ann M. Rose,[4] Stephen C. West,[3] Barbara J. Meyer,[2] Simon J. Boulton[1]†

Meiotic crossovers (COs) are tightly regulated to ensure that COs on the same chromosome are distributed far apart (crossover interference, COI) and that at least one CO is formed per homolog pair (CO homeostasis). CO formation is controlled in part during meiotic double-strand break (DSB) creation in *Caenorhabditis elegans*, but a second level of control must also exist because meiotic DSBs outnumber COs. We show that the anti-recombinase RTEL-1 is required to prevent excess meiotic COs, probably by promoting meiotic synthesis-dependent strand annealing. Two distinct classes of meiotic COs are increased in *rtel-1* mutants, and COI and homeostasis are compromised. We propose that RTEL-1 implements the second level of CO control by promoting noncrossovers.

Homologous recombination repair of meiotic DNA double-strand breaks (DSBs) is regulated to ensure the correct number and placement of meiotic crossovers (COs). One CO per chromosome ensures that homologous chromosomes are held together, can orient toward opposite spindle poles, and thereby segregate correctly at the first meiotic division. Crossover interference (COI) ensures appropriate distribution of COs among chromosomes because the formation of one CO reduces the likelihood of other COs occurring nearby. Meiotic COI is "complete" in *Caenorhabditis elegans*: Only a single CO occurs on each chromosome (*1*, *2*). COI is regulated in part by the condensin I complex, which limits meiotic DSB formation (*3*). Because the average number of meiotic DSBs per chromosome is 2.1 (*3*), and only one of these is repaired as a CO, a second tier of CO control must exist downstream of meiotic DSB formation that channels about half of all DSBs into noncrossovers (NCOs). However, the proteins involved in generating a meiotic CO versus NCO are not well understood.

Human RTEL1 (and *C. elegans* RTEL-1, by homology) negatively regulates recombination by disassembling D loop–recombination intermediates during DNA repair (*4*). If RTEL1 acts similarly on meiotic recombination intermediates, it could be the key protein required to execute NCOs by promoting meiotic synthesis-dependent strand annealing (SDSA). By genetic measurements, recombination in *C. elegans rtel-1* mutants was significantly increased in five genetic intervals on three chromosomes, including both chromosome center and arm regions (Fig. 1A and table S1)

[1]DNA Damage Response Laboratory, London Research Institute, Cancer Research UK, Clare Hall, South Mimms, EN6 3LD, UK. [2]Howard Hughes Medical Institute, Department of Molecular and Cell Biology, University of California at Berkeley, Berkeley, CA 97420, USA. [3]Genetic Recombination Laboratory, London Research Institute, Cancer Research UK, Clare Hall, South Mimms, EN6 3LD, UK. [4]Department of Medical Genetics, Faculty of Medicine, University of British Columbia, Vancouver, BC, V6T 1Z4, Canada.

*Present address: Department of Cellular and Molecular Pharmacology, University of California, San Francisco, San Francisco, CA, 94518–2517, USA.
†To whom correspondence should be addressed. E-mail: simon.boulton@cancer.org.uk

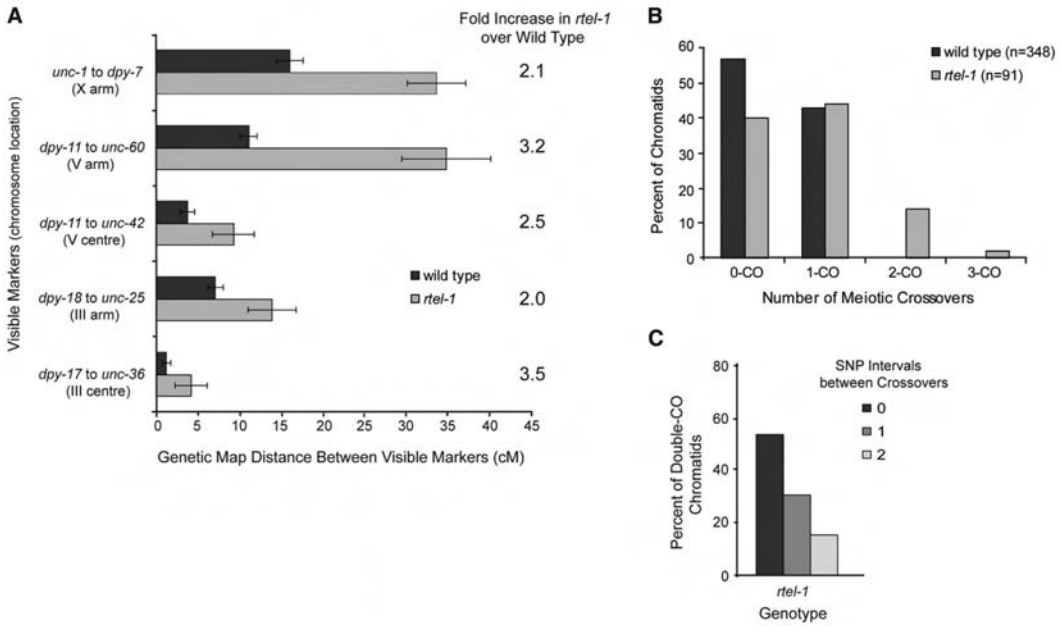

Fig. 1. Recombination is increased in multiple chromosomal regions in *rtel-1* mutants. (**A**) Recombination as measured by genetic map distance (in centimorgans) between pairs of marker genes in wild-type and *rtel-1* mutants. Error bars are 95% CI. (**B**) Percentage of total chromatids (*n*) with no CO or single, double, or triple COs in wild-type and *rtel-1* mutants. (**C**) Number of SNP intervals occurring between COs on double-CO chromatids.

(*4*, *5*). We used five snip–single-nucleotide polymorphisms (snip-SNPs) distributed along 80% of the X chromosome to track recombination events (Fig. 2B). Of wild-type chromatids, 43% had a single CO, and no double COs were observed, as expected (*3*) (Fig. 1B) [normally, 50% of chromatids have a single CO, as one CO occurs per homolog pair (*6*)]. In *rtel-1* mutants, single, double, and triple CO chromatids occurred at a frequency of 44, 14, and 2%, respectively (Figs. 1B and 2B). The number of chromatids with COs in *rtel-1* mutants was significantly different from that of wild type ($P = 1.68e^{-10}$), which indicated that complete COI is defective in the absence of RTEL-1. The 44% of single CO chromatids in *rtel-1* mutants is consistent with the observation that 38% of bivalents receive only one meiotic DSB (*3*). The number of double-CO chromatids in *rtel-1* mutants is also greater than triple-CO chromatids (Figs. 1B and 2B), consistent with the reported distribution of meiotic DSBs (*3*). Therefore, it is possible that all DSBs in *rtel-1* mutants become COs. Examination of the relative positions of COs on double-CO chromatids suggests that there is no interference between multiple COs in *rtel-1* mutants, because double COs occur in adjacent SNP intervals at a frequency that does not differ from random ($P = 1.00$) (Fig. 1C and fig. S1). This lack of interference agrees with the idea that all DSBs in *rtel-1* mutants become COs.

Condensin I complex mutants, such as *dpy-28*, alter the distribution and increase the overall number of COs that occur on each chromosome because of an increase in meiotic DSB formation (*3*, *7*). To determine whether the increased COs seen in *rtel-1* mutants reflect an elevation in recombination precursors (as does *dpy-28*), we measured the number of DSBs generated in *rtel-1* mutants using RAD-51 protein as a marker (*3*). *rtel-1* mutants had slightly more RAD-51 foci, consistent with RTEL-1 having a role in dis-

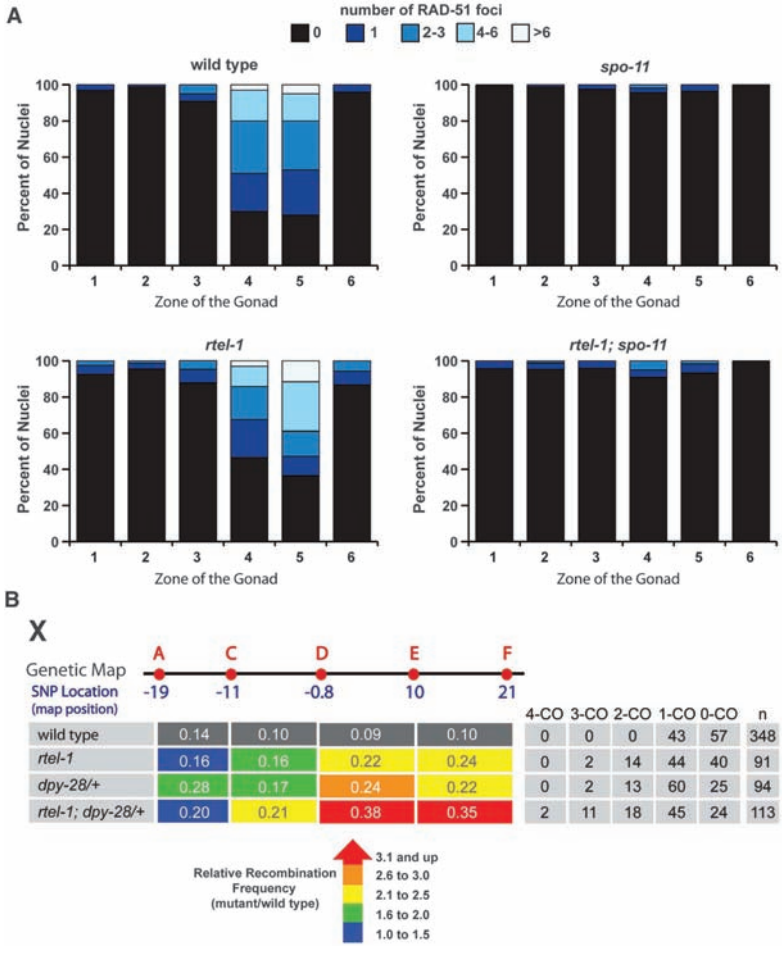

Fig. 2. DSBs are similar in wild-type and *rtel-1* mutants; *rtel-1* and *dpy-28*/+ mutations have an additive effect on CO frequency. (**A**) Number of RAD-51 foci in 100 nuclei in each zone of the gonad for each genotype. Zones are as previously defined (*17*). (**B**) Recombination frequencies measured between SNPs A to C, C to D, D to E, and E to F in each genotype. Relative recombination frequencies in each mutant compared with wild type are by color: blue, 1.0- to 1.5-fold; green, 1.6- to 2.0-fold; yellow, 2.1- to 2.5-fold; orange, 2.6- to 3.0-fold; and red, 3.1-fold increase or greater. The table at right shows the percentage of total chromatids (*n*) with no COs or single, double, triple, or quadruple COs.

assembling unstable D loop–repair intermediates (*4*). The distribution of RAD-51 foci in *rtel-1* mutants, as well as dependence on the DSB formation protein SPO-11, was similar to that of wild type (Fig. 2A and fig. S2). Meiotic DSB formation was also quantified in wild-type and *rtel-1* mutants subject to RNA interference (RNAi) with *rad-54*, which stalls recombination intermediates after RAD-51 loading in yeast (*8*) and *C. elegans* (*3*). No significant difference in RAD-51 foci was observed in *rad-54* RNAi–treated wild-type and *rtel-1* mutants (average wild type, 11.8 ± 3.2 SD; *rtel-1*, 12.2 ± 4.1 SD). Elevated levels of meiotic DSBs generated in the *dpy-28* mutant are sufficient to partially rescue *him-17* mutants, which are deficient in meiotic DSB formation (*7*). Combining the *rtel-1* mutation with either the *spo-11* or *him-17* mutations did not rescue the *spo-11* or *him-17* mutant phenotypes (fig. S3). Unlike *dpy-28* mutants, the elevated COs in *rtel-1* mutants cannot be explained by an increase in CO precursors, which suggests a breakdown at a second level of CO control distinct from DSB formation.

Because RTEL-1 and DPY-28 appear to control CO formation by different means, we examined the effect on recombination of combining *rtel-1* and *dpy-28* mutations. In *dpy-28(s939)*/+ mutants, 60, 13, and 2% of chromatids showed single, double, and triple COs, respectively (*3*) (Fig. 2B). When *rtel-1* mutation was combined with *dpy-28(s939)*/+, quadruple COs were observed in 2% of *rtel-1; dpy-28*/+ mutant chromatids (but were not observed in either single mutant), and 45, 18, and 11% of *rtel-1; dpy-28*/+ mutant chromatids had single, double, and triple COs, respectively (Fig. 2B). Furthermore, 44% of the total measured intervals had a CO in *rtel-1; dpy-28*/+ animals, whereas 32% had a CO in *dpy-28*/+, and 25% had a CO in *rtel-1* mutants. In the *rtel-1; dpy-28*/+ mutant, the total CO frequency was significantly different from that of either single mutant ($P = 0.00014$ for *rtel-1* versus *rtel-1; dpy-28*; $P = 0.0097$ for *dpy-28*/+ versus *rtel-1; dpy-28*/+). Double COs in *rtel-1; dpy-28*/+ double mutants occurred in adjacent SNP intervals at a frequency that did not differ from random ($P = 0.824$), which suggested no residual interference (fig. S1). These data indicate an additive effect of combining *dpy-28*/+ and *rtel-1* mutations on meiotic CO frequency, which supports the hypothesis that RTEL-1 and DPY-28 regulate CO formation through distinct mechanisms. These data also reinforce the idea that all DSBs are converted to COs in the absence of RTEL-1.

Meiotic CO homeostasis in yeast maintains COs at the expense of NCOs under conditions where meiotic DSBs are decreased (*9*, *10*). Conversely, beyond the single "obligate" CO per chromosome, most extra DSBs in *C. elegans* appear to be channeled into NCO pathways, such as SDSA. Given that mutation in *dpy-28* causes an increase in meiotic DSBs (*3*, *7*), the additive effect of *rtel-1* and *dpy-28* mutations on meiotic CO frequency suggested that RTEL-1 may function to maintain homeostasis when there are extra DSBs. If additional meiotic DSBs generated by treatment with ionizing radiation (IR) are repaired predominantly through CO pathways in *rtel-1* mutants, this would lead to increased numbers of COs. Treating *rtel-1* mutants with 10 or 75 Gy of IR resulted in a large, dose-dependent increase in COs, up to 6.7-fold over untreated wild-type animals in the intervals measured, whereas relatively small increases in recombination were observed in wild-type animals after IR (Fig. 3A, fig. S2, and table S2). These data indicate that homeostasis is compromised in the absence of RTEL-1.

During *C. elegans* meiosis, the ZHP-3 protein becomes restricted to recombination foci; one focus per chromosome and six spots per nucleus are observed in wild type (*11*). In wild-type nematodes, only 1% of nuclei had greater than six ZHP-3::GFP (ZHP-3 marked with green fluorescent protein) foci, whereas in *rtel-1* mutants, 18% of nuclei had more than six ZHP-3 foci (Fig. 3, B and C). This was a significant, but relatively small, increase compared with the increased COs observed by our genetic and snip-SNP methods.

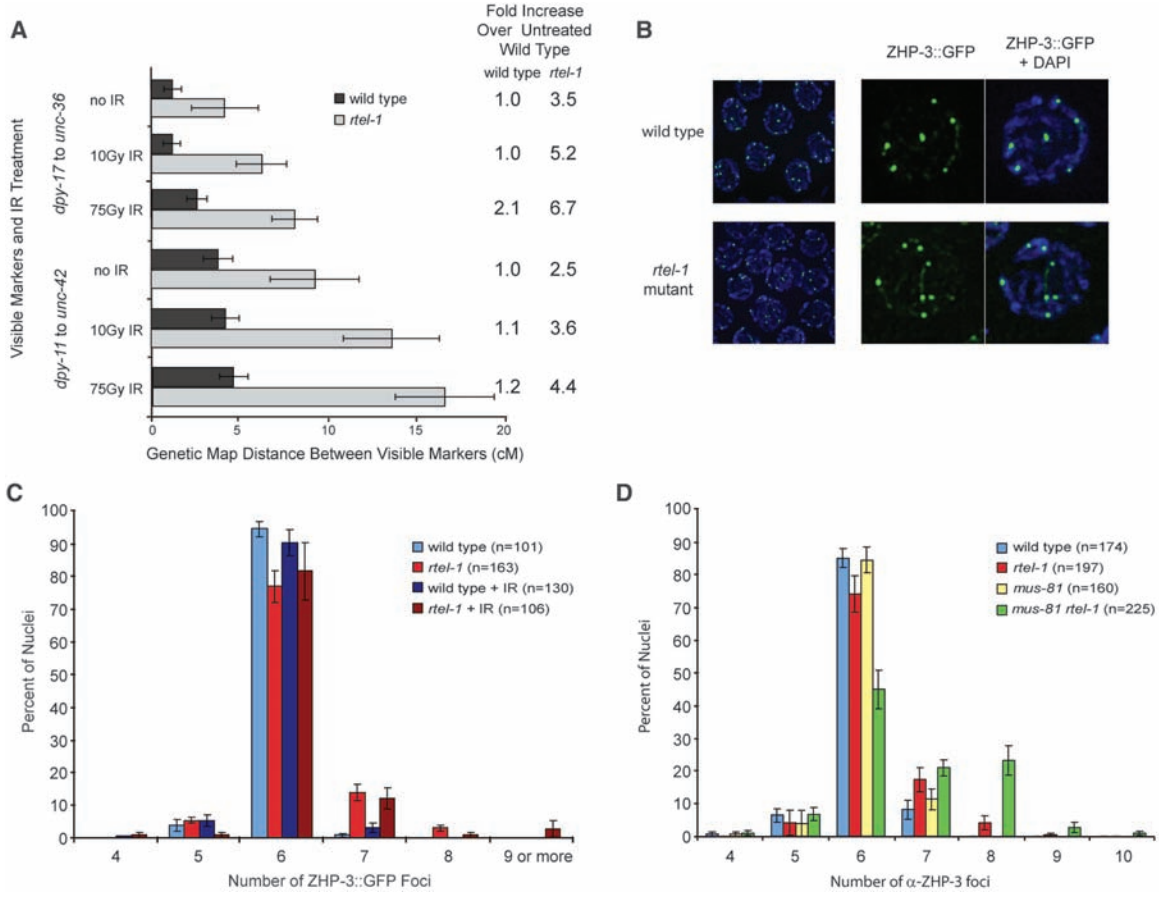

Fig. 3. Recombination increases greatly in *rtel-1* mutants after IR treatment but ZHP-3::GFP foci do not; ZHP-3 foci are increased in *mus-81 rtel-1* mutants. (**A**) Recombination as measured by genetic map distance between pairs of marker genes for two intervals with no IR or 10 or 75 Gy IR in wild-type and *rtel-1* mutants. Fold increase in recombination is compared with untreated wild type. Error bars are 95% CI. (**B**) ZHP-3::GFP foci (green) and 4′,6′-diamidino-2-phenylindole (DAPI)–stained (blue) in wild-type and *rtel-1* mutants at meiotic diplotene. (**C**) Percentage of total nuclei (*n*) with the indicated number of ZHP-3::GFP foci in wild-type and *rtel-1* mutants without treatment and 24 hours after 75 Gy IR. Error bars are SEM. (**D**) Percentage of total nuclei (*n*) with the indicated number of anti–ZHP-3 foci in each genotype. Error bars are SEM.

As recombination greatly increases in *rtel-1* mutants after IR, if ZHP-3 marks all COs, a large increase in ZHP-3 foci should occur after 75 Gy IR. However, ZHP-3 foci remained unchanged in wild-type animals and *rtel-1* mutants after IR (Fig. 3C) [supporting online material (SOM) text]. These data support the hypothesis that ZHP-3 marks only a subset of COs and imply that two classes of meiotic CO events are elevated in *rtel-1* mutants.

In *Saccharomyces cerevisiae*, two classes of COs exist: (i) Those that predominate are dependent on the ZMM proteins (Zip1-4, Mer3, Msh4, and Msh5) and exhibit COI; and (ii) a second class includes those that are independent of the ZMMs, require Mms4 and Mus81, and do not exhibit COI (*12*, *13*). Until now, *C. elegans* was thought to have only class I COs (*14*, *15*). We found COs in the *rtel-1* mutant to fall into two classes: ZHP-3–associated obligate-type COs and COs produced by repair events not associated with ZHP-3 occurring in the absence of RTEL-1. A reliance of COs not associated with ZHP-3 on MUS-81 in *rtel-1* mutants is consistent with the synthetic embryonic lethality of *mus-81 rtel-1* double mutants (*4*). Excess COs generated in wild type after x-ray are similarly dependent on MUS-81 (fig. S4 and SOM text). In *mus-81 rtel-1* double mutants, RAD-51 foci persist (*4*), and ZHP-3 restriction to foci is delayed or does not occur in 65% of nuclei (SOM text), which suggests defects in intermediate processing that may account for the synthetic lethality. In double-mutant nuclei where ZHP-3 foci are observed, foci are increased compared with wild type and with either single mutant (Fig. 3D and SOM text), which indicates that more obligate-type COs are formed in the absence of both RTEL-1 and MUS-81 (fig. S7).

NCO repair of meiotic DSBs in *S. cerevisiae* is thought to occur mainly through the SDSA pathway (*16*). A key step in SDSA is the disruption of the D loop joint molecule. Human RTEL1 can disrupt a preformed D loop in vitro, but the mechanism of RTEL1 action is not well understood (*4*). We considered whether D loop unwinding might require species-specific interactions with RAD51. However, RTEL1 efficiently disrupted D loops preformed by using the *E. coli* RAD51 homolog RecA and single-stranded DNA (ssDNA) binding protein SSB (fig. S5). To determine whether RTEL1 exhibits structural preference for D loops, we generated three substrates: a 3′ ssDNA invasion with a 5′ overhang, a 5′ ssDNA invasion with a 3′ overhang, and a substrate with no overhang. When incubated with RAD51 and replication protein A (RPA), RTEL1 preferentially disrupted the 3′ invasion D loop but showed negligible activity toward D loop substrates with either 5′ invasion or no overhang (Fig. 4, A to C, and fig. S6). Efficient unwinding of the 3′ invasion D loop required incubation with RPA (Fig. 4D). Thus, RTEL1 activity in vitro is consistent with a role in displacing transient strand invasion events in vivo. Taken together, our data support a role for RTEL-1 in meiotic SDSA that enforces COI by preventing further DSBs (beyond the obligate CO) from becoming COs.

In summary, our data support the hypothesis that RTEL-1 regulates meiotic recombination and CO homeostasis in *C. elegans* by physically dissociating strand invasion events and thereby promotes NCO repair by meiotic SDSA (fig. S7). Two levels of meiotic CO control have now been identified in *C. elegans*: regulation of DSB

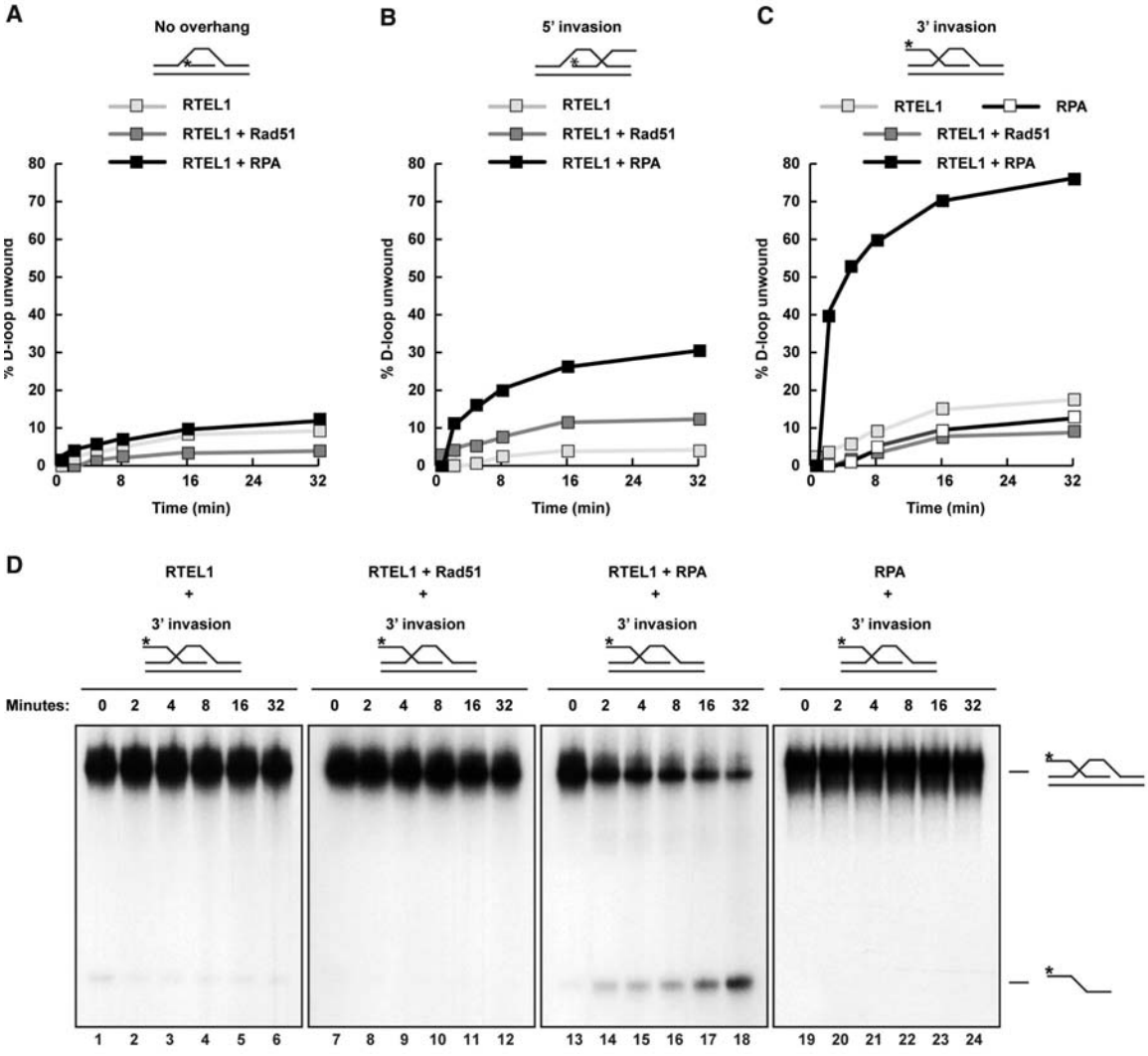

Fig. 4. RTEL1 preferentially dissociates D loops with 3′ invasion and is dependent on RPA. D loop substrates with (**A**) no overhang, (**B**) 5′ invasion, or (**C**) 3′ invasion. Shown is quantification of the percentage of D loop unwound over time. (**D**) Time course of RTEL1 activity toward a D loop substrate with 3′ invasion alone or with the indicated proteins. The fastest migrating band is the displaced radiolabeled (*) ssDNA probe; the slower species is the D loop substrate.

number and distribution by the condensin I complex (*3*) and execution of NCOs by RTEL-1.

References and Notes

1. K. J. Hillers, A. M. Villeneuve, *Curr. Biol.* **13**, 1641 (2003).
2. W. Wood, *The Nematode* Caenorhabditis elegans (Cold Spring Harbor Laboratory Press, Cold Spring Harbor, NY, 1988).
3. D. G. Mets, B. J. Meyer, *Cell* **139**, 73 (2009).
4. L. J. Barber *et al.*, *Cell* **135**, 261 (2008).
5. Materials and methods are available as supporting material on *Science* Online.
6. P. M. Meneely, A. F. Farago, T. M. Kauffman, *Genetics* **162**, 1169 (2002).
7. C. J. Tsai *et al.*, *Genes Dev.* **22**, 194 (2008).
8. B. O. Krogh, L. S. Symington, *Annu. Rev. Genet.* **38**, 233 (2004).
9. E. Martini, R. L. Diaz, N. Hunter, S. Keeney, *Cell* **126**, 285 (2006).
10. S. Y. Chen *et al.*, *Dev. Cell* **15**, 401 (2008).
11. N. Bhalla, D. J. Wynne, V. Jantsch, A. F. Dernburg, R. S. Hawley, *PLoS Genet.* **4**, e1000235 (2008).
12. D. K. Bishop, D. Zickler, *Cell* **117**, 9 (2004).
13. N. M. Hollingsworth, S. J. Brill, *Genes Dev.* **18**, 117 (2004).
14. T. Garcia-Muse, S. J. Boulton, *Chromosome Res.* **15**, 607 (2007).
15. M. Zetka, *Genome Dyn.* **5**, 43 (2009).
16. M. S. McMahill, C. W. Sham, D. K. Bishop, *PLoS Biol.* **5**, e299 (2007).
17. M. P. Colaiácovo *et al.*, *Dev. Cell* **5**, 463 (2003).

18. This work was supported by Cancer Research UK (S.J.B. and S.C.W.) and the Canadian Institute of Health Research (A.M.R.). B.J.M. is an investigator of the Howard Hughes Medical Institute.

Supporting Online Material

www.sciencemag.org/cgi/content/full/327/5970/1254/DC1
Materials and Methods
SOM Text
Figs. S1 to S7
Tables S1 and S2
References

9 October 2009; accepted 28 January 2010
10.1126/science.1183112

Spatially Ordered Dynamics of the Bacterial Carbon Fixation Machinery

David F. Savage,* Bruno Afonso,* Anna H. Chen, Pamela A. Silver†

Cyanobacterial carbon fixation is a major component of the global carbon cycle. This process requires the carboxysome, an organelle-like proteinaceous microcompartment that sequesters the enzymes of carbon fixation from the cytoplasm. Here, fluorescently tagged carboxysomes were found to be spatially ordered in a linear fashion. As a consequence, cells undergoing division evenly segregated carboxysomes in a nonrandom process. Mutation of the cytoskeletal protein ParA specifically disrupted carboxysome order, promoted random carboxysome segregation during cell division, and impaired carbon fixation after disparate partitioning. Thus, cyanobacteria use the cytoskeleton to control the spatial arrangement of carboxysomes and to optimize the metabolic process of carbon fixation.

Efficient cellular metabolism relies on the compartmentalization of enzymatic reactions. Prokaryotes achieve this organization by using capsidlike protein microcompartments to isolate metabolic pathways from the cellular milieu (*1*–*3*). The best-characterized microcompartment, the carboxysome, is found in cyanobacteria and chemoautotrophs and is responsible for catalyzing more than 40% of Earth's carbon fixation (*2*, *4*). Structurally, the carboxysome consists of an icosahedral proteinaceous shell that encloses the enzymes carbonic anhydrase and ribulose-1,5-bisphosphate carboxylase-oxygenase (RuBisCO) (*5*–*8*). The shell may act as a semipermeable barrier, allowing the passive import of the negatively charged reactants, HCO_3^- and ribulose 1,5-bisphosphate, and excluding the competing substrate O_2. Within the carboxysome, carbonic anhydrase catalyzes the production of CO_2, where it is fixed by RuBisCO into 3-phosphoglycerate. Carbon fixation is the basis of biosynthesis in cyanobacteria, and genetic disruption of the carboxysome is lethal (*9*, *10*). Thus, the proper assembly and function of carboxysomes is fundamental to carbon fixation and cellular fitness.

We developed methods to visualize carboxysomes and to investigate their dynamical behavior in living cells. The carboxysome consists of ~5000 monomers of the shell protein CcmK and ~2000 monomers of RuBisCO (*5*). Expression of these proteins in the cyanobacterium *Synechococcus elongatus* PCC7942 (hereafter *Synechococcus*) (*11*) fused to green, yellow, or cyan fluorescent protein (GFP, YFP, or CFP) yielded fluorescent particles, and the proteins colocalized when coexpressed in the same cell, which indicated assembled carboxysomes (Fig. 1A). The labeled carboxysomes also contained endogenous RuBisCO (Fig. 1B). Electron microscopy showed that all carboxysomes contain RbcL-GFP and that all RbcL-GFP was in carboxysomes (Fig. 1C). Carboxysome morphology and cellular growth rates were unaffected by YFP fusions (fig. S1).

Carboxysomes were evenly spaced along the long axis of *Synechococcus* (Fig. 2A). On average, there were 3.7 ± 1.2 carboxysomes per cell under log phase growth (Fig. 2B). We calculated the pairwise distances between carboxysomes in cells (n = 2508) with four carboxysomes (Fig. 2C). The average spacing between adjacent carboxysomes was 0.66 μm but was proportional to cell length (Fig. 2D). Thus, normalizing by cell length sharpened the pair-

Department of Systems Biology, Harvard Medical School, Boston, MA 02115, USA.

*These authors contributed equally to this work.
†To whom correspondence should be addressed. E-mail: pamela_silver@hms.harvard.edu

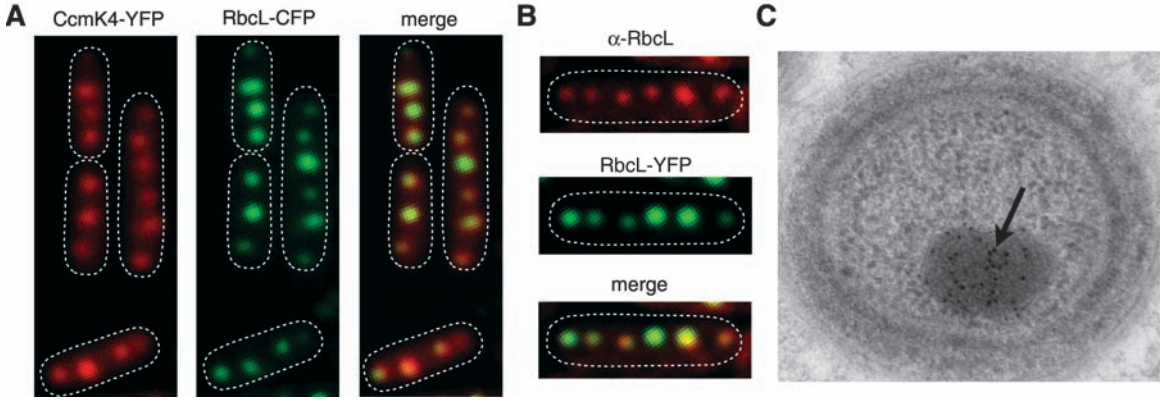

Fig. 1. The carboxysome can be fluorescently labeled. (**A**) Fluorescence colocalization of shell protein CcmK4-YFP and RuBisCO protein RbcL-CFP. (**B**) Immunofluorescence microscopy with an antibody against RuBisCO as a probe and showing RbcL-YFP colocalized to cytoplasmic RuBisCO. (**C**) Transverse cell electron micrograph showing, by means of immunogold labeling with an antibody against GFP, localization of RbcL-GFP to carboxysomes.